arXiv:nucl-ex/9909016v1 27 Sep 1999

Model-independent determination of the ^{12}C$(p,p')^{12}$C* (15.11 MeV, 1^+, T=1) transition amplitude at 200 MeV

S. P. Wells* and S. W. Wissink
Indiana University Cyclotron Facility, Bloomington, Indiana 47408

(February 8, 2008)

Abstract

Using data obtained through simultaneous measurements of $(\vec{p},\vec{p}\,')$ spin-transfer observables and $(\vec{p},p'\gamma)$ coincident spin observables, we have made a model-independent determination of the complete scattering amplitude for the 15.11 MeV, 1^+, T=1 state in ^{12}C at an incident proton energy of 200 MeV, for four proton scattering angles ranging from $\theta_{\text{c.m.}} = 5.5^\circ$ to 16.5°. At each angle, 16 different observables were determined, whereas only 11 independent quantities are required to specify the transition amplitude for this state. It had been shown previously that the set of observables measured span the allowed space; hence the system is overdetermined, which allowed us to extract, in a model-independent fashion, each of the individual spin-operator amplitudes that characterize the reaction. Additional insight into the physical mechanisms that drive this transition is obtained by mapping out the momentum-transfer dependence of these amplitudes. We also compare the magnitudes and phases determined for each of the spin-operator amplitudes to the predictions of calculations performed in both relativistic and nonrelativistic frameworks, and discuss the physics content of these comparisons.

25.40.Ep, 24.70.+s, 25.90.+k

Typeset using REVTEX

I. INTRODUCTION

At intermediate energies of ∼150–500 MeV, hadron-induced nuclear reactions have served as a rich source of information, both to further our understanding of nuclear structure, and to illustrate how the elementary nucleon-nucleon (NN) interaction may be modified in the nuclear medium [1]. This is particularly true of spin observables, which often contain contributions from interferences between different pieces of the full scattering amplitude. These interferences, inaccessible through measurements of differential cross sections alone, can thus provide information about not only the magnitudes, but also the relative phases of individual terms in the transition amplitude. Ideally, one would like to extract precise values for each of these (complex) terms in a manner which does not rely on specific model assumptions. This information, in turn, can then provide the most stringent tests of a given theoretical prediction for the hadronic process of interest.

To obtain deeper insight into the nucleon-nucleus (NA) interaction, several inelastic transitions have been identified as being particularly amenable to experimental investigation. The strong, isovector 1^+ state in ^{12}C at an excitation energy of 15.11 MeV has been extensively studied, using a variety of probes operating under a broad range of kinematic conditions. Due to its 1^+ nature, hadronic excitation of this state represents an "unnatural parity" transition; consequently, this process should be particularly sensitive to the spin-dependent parts of the NA interaction, and in fact has long served as a critical test for our understanding of the $\Delta S = \Delta T = 1$ component of the NN effective interaction [2]. As an example, the spin observable $P - A_y$, i.e., the difference between the polarization induced in the outgoing proton and the scattering yield asymmetry that results from use of a polarized incident beam, has been investigated both experimentally [3,4] and theoretically [5]. This quantity, which in a non-relativistic framework contains only interference terms between competing pieces of the transition amplitude, has been shown to be sensitive to the coupling of the nucleon spin to the bound nucleon current [5]. In later relativistic treatments of proton-nucleus scattering [6,7], it became clear that these same nuclear current terms appear more naturally in a relativistic formalism, and are produced through the linear couplings between the upper and lower components of the bound nucleon wave function [6,7]. In either description, $P - A_y$ is dependent on the momentum of the nucleons inside the nucleus, and is therefore sensitive to the off-shell behavior of these nucleons, and the non-local or exchange nature of the interaction.

Thus, detailed comparisons of measured spin observable data to various predictions for specific nuclear transitions has traditionally been our best means of constraining theoretical models. In recent years, though, such comparisons have raised a number of concerns, at both the experimental and theoretical ends. For example, it has been shown [8,9] that in a direct-only plane-wave impulse approximation (PWIA), certain combinations of $(\vec{p}, \vec{p}\,')$ spin-transfer observables are directly related to individual terms in the effective NN interaction, weighted by corresponding nuclear response functions. When physical processes such as distortion of the projectile waves and knock-on exchange are included, however, it becomes less clear what these combinations of $(\vec{p}, \vec{p}\,')$ observables represent physically, thereby blurring any simple interpretation of these quantities. On the experimental side, counting arguments show that even "complete" sets of $(\vec{p}, \vec{p}\,')$ spin-transfer measurements provide (at most) eight independent pieces of information, while a transition of the general form $0^+ \rightarrow J^\pi$

requires knowledge of $(8J+3)$ independent quantities in order to fully specify the scattering amplitude.

To reduce this ambiguity, it is clearly desirable to establish a more direct connection between theory and experiment, such as would be obtained from a model-independent extraction of individual elements of the scattering amplitude. In so doing, one bypasses the 'intermediate' role played by spin observables, which represent non-trivial combinations of many of these elements. Carrying out such a program, though, requires access to information beyond that provided by $(\vec{p},\vec{p}\,')$ spin-transfer measurements alone. In particular, one must probe the polarization state of the 'other particle' involved in the reaction: the recoil nucleus. This can be achieved through study of the angular correlation in the final state between the scattered (out-going) proton and the particle(s) emitted in the decay of the excited nucleus, as in reactions of the type $(\vec{p},p'\gamma)$. More specifically, for proton excitation of a $0^+ \rightarrow 1^+$ transition, followed by electromagnetic decay back to the ground state, it has recently been proven formally [10,11] that certain $(\vec{p},p'\gamma)$ measurements, when combined with complete sets of $(\vec{p},\vec{p}\,')$ observables, allow for a complete description of the transition amplitude. Note that in this case a total of $8J+3=11$ independent quantities must be determined.

In this paper, we report the first model-independent determination of the complete transition amplitude for any nuclear final state with $J \neq 0$. This analysis is based on a detailed set of measurements [12] carried out at the Indiana University Cyclotron Facility (IUCF), in which both $(\vec{p},\vec{p}\,')$ spin-transfer and $(\vec{p},p'\gamma)$ coincident observables were determined simultaneously for excitation of the isovector 1^+ state at 15.11 MeV in ^{12}C. Data were taken at four proton scattering angles ($\theta_{\mathrm{c.m.}} = 5.5^\circ$, 8.8°, 12.1°, and 16.5°) at an incident proton beam energy of 200 MeV. As will be shown below, this data set allows for extraction of each individual (complex) spin-dependent term in the transition amplitude in a model-independent manner. Moreover, because this procedure has been applied at a number of scattering angles, the momentum-transfer (q) dependence of each spin-operator amplitude has been mapped out, allowing for a clearer interpretation of the physical mechanisms that drive this transition.

This paper will be organized in the following way. In Sec. II we present the formalism adopted (from Ref. [10]) for analysis of the data. In Sec. III, we present the observables measured in the IUCF experiment [12], and express each of these in terms of real and imaginary parts of the individual spin-operator amplitudes. We describe in detail the procedure used to extract these amplitudes from the observables in Sec. IV, and present the results of this procedure in Sec. V. Section VI provides a detailed discussion of the momentum-transfer dependence determined for each amplitude (both magnitude and phase), and compares our results to predictions of calculations performed in both relativistic and nonrelativistic formalisms. Where possible, we discuss the specific physics issues to which each amplitude is sensitive. Our most significant results and conclusions are summarized in Sec. VII.

II. FORMALISM

The formalism adopted here follows that of Piekarewicz *et al.* [10], and has been presented in detail in Ref. [12]; only the most important results are given here for completeness. We work in the orthogonal coordinate system defined by

$$\mathbf{n} \equiv \mathbf{p} \times \mathbf{p}' \ ; \qquad \mathbf{K} \equiv \mathbf{p} + \mathbf{p}' \ ; \qquad \mathbf{q} \equiv \mathbf{n} \times \mathbf{K} \ , \tag{1}$$

where $\mathbf{p}$ ($\mathbf{p}'$) is the incident (outgoing) proton momentum, $\mathbf{n}$ is directed normal to the scattering plane, $\mathbf{K}$ is along the direction of the average proton momentum, and (neglecting the reaction Q-value) $\mathbf{q}$ points in the direction of momentum transfer $\mathbf{p}'$–$\mathbf{p}$. In this frame, the most general form of the scattering amplitude allowed by angular momentum and parity conservation for a $0^+ \to 1^+$ transition can be written in the form [10]

$$\begin{aligned} \hat{T}^p(\mathbf{p},\mathbf{p}') \ = \ & A_{n0}(\hat{\mathbf{\Sigma}} \cdot \hat{\mathbf{n}}) \ + \ A_{nn}(\hat{\mathbf{\Sigma}} \cdot \hat{\mathbf{n}})(\sigma \cdot \hat{\mathbf{n}}) \ + \ A_{KK}(\hat{\mathbf{\Sigma}} \cdot \hat{\mathbf{K}})(\sigma \cdot \hat{\mathbf{K}}) \\ & + \ A_{Kq}(\hat{\mathbf{\Sigma}} \cdot \hat{\mathbf{K}})(\sigma \cdot \hat{\mathbf{q}}) \ + \ A_{qK}(\hat{\mathbf{\Sigma}} \cdot \hat{\mathbf{q}})(\sigma \cdot \hat{\mathbf{K}}) \ + \ A_{qq}(\hat{\mathbf{\Sigma}} \cdot \hat{\mathbf{q}})(\sigma \cdot \hat{\mathbf{q}}) \ , \end{aligned} \tag{2}$$

where

$$\hat{\mathbf{\Sigma}}_M \ \equiv \ |1^+M\rangle\langle 0^+| \tag{3}$$

is the polarization operator for promoting a 0^+ state to a state with $J^\pi{=}1^+$ and magnetic substate M, while $\vec{\sigma}$ are the Pauli spin operators for the projectile. In Eq. 2, the $A_{i\mu}$'s are scalar functions of energy and momentum transfer, where the subscripts $i(= n, K, q)$ and $\mu(= 0, n, K, q)$ indicate the polarization components of the recoil 1^+ nucleus ($\mathbf{\Sigma}$) and the scattered proton ($\vec{\sigma}$, with $\sigma_0 \equiv 1$), respectively. Because there are six allowed complex amplitudes, 11 pieces of information (after eliminating one overall phase) are required to specify the scattering amplitude for this transition.

If the final polarization of the nuclear state is undetected, one can sum incoherently over the $\mathbf{\Sigma}$ index. In this case, the relevant spin observables can be expressed as

$$\begin{aligned} \frac{d\sigma}{d\Omega_p} \ &= \ \sum_{ij\mu} A_{i\mu} A^*_{j\mu} \delta_{ij} \ , \\ \frac{d\sigma}{d\Omega_p} D_{\alpha\beta} \ &= \ \sum_{ij\mu\nu} A_{i\mu} A^*_{j\nu} \delta_{ij} \frac{1}{2} Tr\{\sigma_\alpha \sigma_\mu \sigma_\beta \sigma_\nu\} \ , \end{aligned} \tag{4}$$

where $\alpha, \beta = 0, n, K, q$. Using the scattering amplitude of Eq. 2 and carrying through the Pauli algebra, it is easily shown that only eight of the 16 possible singles $(\vec{p}, \vec{p}')$ spin observables (the $D_{\alpha\beta}$) are nonzero. Because 11 independent quantities appear in $\hat{T}^p(\mathbf{p},\mathbf{p}')$, one sees that singles measurements alone can not uniquely define this amplitude; or, put another way, there is information contained in $\hat{T}^p(\mathbf{p},\mathbf{p}')$ which is not accessible via $(\vec{p}, \vec{p}')$ observables. In particular, the presence in Eq. 4 of the Kronecker δ_{ij} makes it impossible to determine the relative phase between any two spin operator amplitudes ($A_{i\mu}$'s) that correspond to orthogonal orientations of the recoil nuclear polarization.

If one makes the assumption that the $(p, p'\gamma)$ reaction is strictly a two-step process, then the total transition amplitude (excitation plus decay) can be written as the product of the strong and electromagnetic amplitudes. In this case, all of the coincident $(p, p'\gamma)$ observables may be written in terms of just the singles (p, p') spin operator amplitudes, $A_{i\mu}$, and the γ-ray branching ratio to the ground state R [10]. In complete analogy with the singles observables (Eq. 4), the spin-dependent coincident observables for this transition can be written in the form [10]

$$
\begin{aligned}
\frac{d^2\sigma}{d\Omega_p d\Omega_\gamma}(\hat{\mathbf{k}}) &= \frac{3R}{8\pi}\sum_{ij\mu} A_{i\mu}A^*_{j\mu}t_{ij}(\hat{\mathbf{k}}) \ , \\
\frac{d^2\sigma}{d\Omega_p d\Omega_\gamma}(\hat{\mathbf{k}})D_{\alpha\beta}(\hat{\mathbf{k}}) &= \sum_{ij\mu\nu} A_{i\mu}A^*_{j\nu}t_{ij}(\hat{\mathbf{k}})\,\frac{1}{2}Tr\{\sigma_\alpha\sigma_\mu\sigma_\beta\sigma_\nu\} \ ,
\end{aligned}
\tag{5}
$$

where $\hat{\mathbf{k}}$ is the momentum direction of the emitted photon, and the photon polarization tensor t_{ij} is given by

$$
t_{ij}(\hat{\mathbf{k}}) \equiv \delta_{ij} - (\hat{\mathbf{k}}\cdot\hat{\mathbf{e}}_i)(\hat{\mathbf{k}}\cdot\hat{\mathbf{e}}_j) \ , \tag{6}
$$

with $\hat{\mathbf{e}}_i$ a unit vector lying along one of the $(\hat{\mathbf{n}}, \hat{\mathbf{K}}, \hat{\mathbf{q}})$ coordinates defined in Eq. 1. It is important to emphasize that the coincident observables defined in Eq. 5 are written in terms of the *same* $A_{i\mu}$'s that appear in the definitions of the singles observables, Eq. 4. The crucial difference between these two sets of equations is the presence of $t_{ij}(\hat{\mathbf{k}})$ in the definition of the coincident observables, replacing the δ_{ij} for the singles observables. Thus, certain $(p, p'\gamma)$ spin observables *will* be sensitive to the relative phases between amplitudes for different recoil nuclear polarizations, provided that the emitted γ–ray has momentum components along *both* $\hat{\mathbf{e}}_i$ and $\hat{\mathbf{e}}_j$. Thus, the specific information about the transition amplitude which is lost for the singles observables can be accessed through coincident $(\vec{p}, p'\gamma)$ measurements.

III. SUMMARY OF OBSERVABLES

In this paper, we present detailed analysis of the data from a previous experiment [12]. In that work, some spin observables were measured using an incident proton beam whose polarization vector was normal to the (horizontal) scattering plane, while others required use of a beam in which the polarization vector had been precessed to lie in the scattering plane. Due to technical problems encountered during data acquisition [12], reliable values of the differential cross section, $d\sigma/d\Omega_p$, could not be extracted from the experimental yields. While this problem had no effect on the determination of spin-dependent observables, it was necessary to use previously measured values of $d\sigma/d\Omega_p$ for this transition [13] to set the scale for the overall magnitudes of the $A_{i\mu}$ amplitudes. In this paper, these amplitudes will be presented in units of $\sqrt{\mu\text{b/sr}}$.

The singles observables obtained in Ref. [12] include the three normal-component spin-transfer coefficients A_y, P, and $D_{N'N}$, and two linear combinations of the in-plane spin transfer coefficients,

$$
\begin{aligned}
D_\lambda &\equiv D_{L'L}\sin\alpha + D_{S'L}\cos\alpha \ , \\
D_\sigma &\equiv D_{L'S}\sin\alpha + D_{S'S}\cos\alpha \ ,
\end{aligned}
\tag{7}
$$

where here α is the spin precession angle about $\hat{\mathbf{n}}$ experienced by the scattered protons in passing through the magnetic spectrometer used in the experiment. Through use of Eq. 4, all of these measured $(\vec{p}, \vec{p}\,')$ observables can be expressed in terms of the $A_{i\mu}$ amplitudes as follows:

$$
\begin{aligned}
\frac{d\sigma}{d\Omega_p} &= |A_{n0}|^2 + |A_{nn}|^2 + |A_{KK}|^2 + |A_{Kq}|^2 + |A_{qK}|^2 + |A_{qq}|^2 \ , \\
\frac{d\sigma}{d\Omega_p} A_y &= 2[\Re(A_{n0}A^*_{nn}) + \Im(A_{KK}A^*_{Kq} + A_{qK}A^*_{qq})] \ , \\
\frac{d\sigma}{d\Omega_p} P &= 2[\Re(A_{n0}A^*_{nn}) - \Im(A_{KK}A^*_{Kq} + A_{qK}A^*_{qq})] \ , \\
\frac{d\sigma}{d\Omega_p} D_{N'N} &= |A_{n0}|^2 + |A_{nn}|^2 - |A_{KK}|^2 - |A_{Kq}|^2 - |A_{qK}|^2 - |A_{qq}|^2 \ ; \qquad (8)
\end{aligned}
$$

and

$$
\begin{aligned}
\frac{d\sigma}{d\Omega_p} D_\lambda &= \cos\theta_{pK}[\sin(\alpha - \theta_{\text{c.m.}} + \theta_{pK})\frac{d\sigma}{d\Omega_p} D_{KK} + \cos(\alpha - \theta_{\text{c.m.}} + \theta_{pK})\frac{d\sigma}{d\Omega_p} D_{qK}] \\
&- \sin\theta_{pK}[\sin(\alpha - \theta_{\text{c.m.}} + \theta_{pK})\frac{d\sigma}{d\Omega_p} D_{Kq} + \cos(\alpha - \theta_{\text{c.m.}} + \theta_{pK})\frac{d\sigma}{d\Omega_p} D_{qq}] \ , \\
\frac{d\sigma}{d\Omega_p} D_\sigma &= \sin\theta_{pK}[\sin(\alpha - \theta_{\text{c.m.}} + \theta_{pK})\frac{d\sigma}{d\Omega_p} D_{KK} + \cos(\alpha - \theta_{\text{c.m.}} + \theta_{pK})\frac{d\sigma}{d\Omega_p} D_{qK}] \\
&+ \cos\theta_{pK}[\sin(\alpha - \theta_{\text{c.m.}} + \theta_{pK})\frac{d\sigma}{d\Omega_p} D_{Kq} + \cos(\alpha - \theta_{\text{c.m.}} + \theta_{pK})\frac{d\sigma}{d\Omega_p} D_{qq}] \ , \qquad (9)
\end{aligned}
$$

where $\theta_{\text{c.m.}}$ is the proton center-of-mass scattering angle, θ_{pK} is the angle between the incident beam momentum $\mathbf{p}$ and the average momentum $\mathbf{K}$ (see Eq. 1), and α is the spin precession angle defined above. The $D_{\alpha\beta}$ spin transfer coefficients that appear in the previous equation can also be expressed in terms of the spin operator amplitudes as:

$$
\begin{aligned}
\frac{d\sigma}{d\Omega_p} D_{KK} &= |A_{n0}|^2 - |A_{nn}|^2 + |A_{KK}|^2 - |A_{Kq}|^2 + |A_{qK}|^2 - |A_{qq}|^2 \ , \\
\frac{d\sigma}{d\Omega_p} D_{Kq} &= -2[\Im(A_{n0}A^*_{nn}) - \Re(A_{KK}A^*_{Kq} + A_{qK}A^*_{qq})] \ , \\
\frac{d\sigma}{d\Omega_p} D_{qK} &= 2[\Im(A_{n0}A^*_{nn}) + \Re(A_{KK}A^*_{Kq} + A_{qK}A^*_{qq})] \ , \\
\frac{d\sigma}{d\Omega_p} D_{qq} &= |A_{n0}|^2 - |A_{nn}|^2 - |A_{KK}|^2 + |A_{Kq}|^2 - |A_{qK}|^2 + |A_{qq}|^2 \ . \qquad (10)
\end{aligned}
$$

For the coincident $(\vec{p}, p'\gamma)$ measurements, the incident beam polarization was either pointed along the normal $\hat{\mathbf{n}}$ to the scattering plane, or was rotated to lie *in* the scattering plane. During vertical polarization running, three photon detectors were positioned in the scattering plane on beam right, and one was placed directly above the target [12]. If a sum over the two beam spin states was performed (effectively producing the results that would be obtained with an unpolarized beam), the coincident yields from the three in-plane detectors could be used to extract the in-plane double-differential cross section, which takes the form [10]

$$
\frac{8\pi}{3R}\frac{d^2\sigma}{d\Omega_\gamma d\Omega_p}(\theta_\gamma) = A(\theta_p) + B(\theta_p)\cos 2\theta_\gamma + C(\theta_p)\sin 2\theta_\gamma \ , \qquad (11)
$$

where R is again the γ-ray branching ratio to the ground state, θ_γ is the photon angle in the scattering plane, measured with respect to the $\hat{\mathbf{q}}$ direction, and A, B, and C are unknown functions of the proton scattering angle. These can be written in terms of amplitudes as:

$$\begin{aligned} A &= |A_{n0}|^2 + |A_{nn}|^2 + \frac{1}{2}[|A_{KK}|^2 + |A_{Kq}|^2 + |A_{qK}|^2 + |A_{qq}|^2] \ , \\ B &= \frac{1}{2}[|A_{KK}|^2 + |A_{Kq}|^2 - |A_{qK}|^2 - |A_{qq}|^2] \ , \\ C &= -\Re[A_{KK}A^*_{qK} + A_{Kq}A^*_{qq}] \ . \end{aligned} \tag{12}$$

We point out that in this work our definitions of A, B, and C do not include the branching ratio normalization factor $8\pi/(3R)$, and are therefore different from the definitions given in Ref. [10]. A more important comment is that, in order to eliminate any sensitivity to detection efficiency in the photon detectors, only the *ratios* of the symmetric and antisymmetric pieces of the in-plane coincident cross section, B/A and C/A, were used in our determination of the transition amplitude. These quantities have the obvious advantage of being independent of any overall normalization error.

We now turn to the spin-dependent coincident observables which, at a given proton scattering angle θ_p, will be functions of the angle θ_γ at which the photon is emitted. If the photon is emitted in the scattering plane, then the normal-component coincident analyzing power, scaled by the coincident cross section, can be cast in a form similar to that of Eq. 11, i.e.,

$$\frac{8\pi}{3R}\frac{d^2\sigma}{d\Omega_\gamma d\Omega_p}(\theta_\gamma)A_y(\theta_\gamma) \ = \ \epsilon_A(\theta_p) + \epsilon_B(\theta_p)\cos 2\theta_\gamma + \epsilon_C(\theta_p)\sin 2\theta_\gamma \ , \tag{13}$$

where

$$\begin{aligned} \epsilon_A &= 2\Re(A_{n0}A^*_{nn}) + \Im(A_{KK}A^*_{Kq} + A_{qK}A^*_{qq}) \ , \\ \epsilon_B &= \Im(A_{KK}A^*_{Kq} - A_{qK}A^*_{qq}) \ , \\ \epsilon_C &= -\Im(A_{KK}A^*_{qq} - A_{Kq}A^*_{qK}) \ , \end{aligned} \tag{14}$$

and $d^2\sigma/d\Omega_\gamma d\Omega_p$ is given by Eqs. 11 and 12. Note that with three values measured for the normal-component spin asymmetry (corresponding to the three angles of the photon detectors), we have three expressions from which the coefficients ϵ_A, ϵ_B, and ϵ_C can be determined. Although this inversion is possible in principle, it is more efficient to use the measured asymmetries directly in our fitting procedure to determine the independent $A_{i\mu}$'s, which we describe in the next section.

With a normally-polarized beam, the photon detector directly above the target could measure another piece of the normal-component coincident analyzing power, given by

$$\frac{d^2\sigma}{d\Omega_\gamma d\Omega_p}(\hat{\mathbf{n}})A_y(\hat{\mathbf{n}}) \ = \ 2\Im(A_{KK}A^*_{Kq} + A_{qK}A^*_{qq}) \ , \tag{15}$$

where

$$\frac{d^2\sigma}{d\Omega_\gamma d\Omega_p}(\hat{\mathbf{n}}) \ = \ |A_{KK}|^2 + |A_{Kq}|^2 + |A_{qK}|^2 + |A_{qq}|^2 \ . \tag{16}$$

It can be shown algebraically that the ratio of Eqs. 15 and 16 can be expressed in terms of the normal-component *singles* observables in the form

$$A_y(\hat{\mathbf{n}}) \;=\; -\,\frac{(P - A_y)}{(1 - D_{N'N})}\;. \tag{17}$$

In Ref. [12] this equation was used to demonstrate that the independently measured $(\vec{p}, p'\gamma)$ coincident and $(\vec{p}, \vec{p}\,')$ singles observables were internally consistent.

Finally, the four remaining $(\vec{p}, p'\gamma)$ observables were extracted from the spin asymmetries measured when the incident beam polarization had been oriented to lie in the scattering plane. These are components of the longitudinal and sideways analyzing powers, $D_{0L}(\hat{\mathbf{k}})$ and $D_{0S}(\hat{\mathbf{k}})$, respectively. These quantities, which vanish identically for singles measurements, are related to the corresponding center-of-mass asymmetries $D_{0K}(\hat{\mathbf{k}})$ and $D_{0q}(\hat{\mathbf{k}})$ via a rotation in the reaction plane through the angle θ_{pK}:

$$\begin{pmatrix} D_{0L}(\hat{\mathbf{k}}) \\ D_{0S}(\hat{\mathbf{k}}) \end{pmatrix} \;=\; \begin{pmatrix} \cos\theta_{pK} & -\sin\theta_{pK} \\ \sin\theta_{pK} & \cos\theta_{pK} \end{pmatrix} \begin{pmatrix} D_{0K}(\hat{\mathbf{k}}) \\ D_{0q}(\hat{\mathbf{k}}) \end{pmatrix}, \tag{18}$$

with $D_{0K}(\hat{\mathbf{k}})$ and $D_{0q}(\hat{\mathbf{k}})$ defined by

$$\begin{aligned}
\frac{8\pi}{3R}\frac{d^2\sigma}{d\Omega_p d\Omega_\gamma}(\hat{\mathbf{k}})D_{0K}(\hat{\mathbf{k}}) \;&=\; 2[\Re(A_{n0}A^*_{KK}) - \Im(A_{nn}A^*_{Kq})]t_{nK}(\hat{\mathbf{k}}) \\
&+\; 2[\Re(A_{n0}A^*_{qK}) - \Im(A_{nn}A^*_{qq})]t_{nq}(\hat{\mathbf{k}})\;, \\
\frac{8\pi}{3R}\frac{d^2\sigma}{d\Omega_p d\Omega_\gamma}(\hat{\mathbf{k}})D_{0q}(\hat{\mathbf{k}}) \;&=\; 2[\Re(A_{n0}A^*_{Kq}) + \Im(A_{nn}A^*_{KK})]t_{nK}(\hat{\mathbf{k}}) \\
&+\; 2[\Re(A_{n0}A^*_{qq}) + \Im(A_{nn}A^*_{qK})]t_{nq}(\hat{\mathbf{k}})\;.
\end{aligned} \tag{19}$$

The four coefficients of $t_{nK}(\hat{\mathbf{k}})$ and $t_{nq}(\hat{\mathbf{k}})$ that appear in the above expressions (i.e., these four combinations of the $A_{i\mu}$'s) can be viewed as independent observables, and were determined in Ref. [12] by a fit to the dual sinusoidal dependence of the measured asymmetries on both the outgoing photon direction $\hat{\mathbf{k}}$ and the orientation of the incident proton polarization in the scattering plane. Contained in these four observables are clear sensitivities to the relative phases between terms in the transition amplitude corresponding to proton and recoil nuclear polarization projections that are normal to, and oriented in, the reaction plane; relative phases which, by virtue of Eq. 4, are inaccessible via singles $(\vec{p}, \vec{p}\,')$ measurements.

IV. MINIMIZATION PROCEDURES

In the set of combined $(\vec{p}, \vec{p}\,')$ and $(\vec{p}, p'\gamma)$ observables discussed above, we have a total of 16 measured quantities at each proton scattering angle, which can be used to determine the 11 independent quantities required to specify the complete scattering amplitude. Although it has been shown formally [11] that certain combinations of these observables can provide an analytic solution of this problem (via matrix inversion), this method of analysis has several disadvantages in practice. Because only particular linear combinations of the measured quantities are used, some statistical information is invariably lost in this method. Of more concern is the loss of any statistical gauge of the quality or internal consistency of the amplitude extraction procedure; because one will always obtain an 'answer,' the assignment of errors to the $A_{i\mu}$ amplitudes becomes somewhat ambiguous.

In this work, *all* of the observables measured at each scattering angle are used as input to a single χ^2 minimization procedure. This method not only makes use of the full statistical information contained in the data set, but also minimizes any bias that could be introduced through data manipulation (e.g., forming various linear combinations of the data) prior to the actual fitting. Thus, our approach can be viewed conceptually as the following: we seek values for the six complex amplitudes $A_{i\mu}$ contained in Eq. 2 that, when used to form the 16 combinations provided in Section II, minimize the differences between these combinations and the measured values of the corresponding observables. Details of the minimization procedure we followed will be provided in the next few paragraphs, but we first point out a few subtle features unique to this problem. Because the amplitudes are complex, one can seek values for either their magnitudes and phases, or for their real and imaginary components. In this work, we carried out independent fits to both parameter sets, and obtained (as one would hope) equivalent results. However, it became clear that when attempting to resolve various discrete ambiguities in the fitting results, or invoking arguments of 'smoothness' (in momentum transfer), use of magnitudes and phases as the fitting parameters was favored. It was also necessary to hold one phase fixed during the fitting, as the observables are insensitive to any uniform shift in all the phases. Because $|A_{nn}|$ was consistently one of the largest magnitudes over the entire angular range studied, we chose to define A_{nn} to be real and positive, and thus determined (in effect) the phase of every other $A_{i\mu}$ relative to that of A_{nn}.

A final choice which required careful thought was the selection of appropriate starting values for the parameters to be fit. To avoid any bias, we noted that the form of the singles cross section, $d\sigma/d\Omega_p$ (Eq. 8), reveals that the maximum allowed value for the magnitude of any of the $A_{i\mu}$'s is constrained by

$$|A_{i\mu}| \leq \sqrt{\frac{d\sigma}{d\Omega_p}} \ . \tag{20}$$

Thus, the allowed parameter space for the magnitudes must be restricted to this range. In our fitting, we therefore assigned starting values for each $|A_{i\mu}|$ by using a linear random number generator to select a number between zero and this maximum. Similarly, starting values for each phase were chosen at random over the allowed range

$$0 \leq \phi_{i\mu} \leq 2\pi \ . \tag{21}$$

By holding ϕ_{nn} at zero, then searching the 11-dimensional parameter space for minima in χ^2, we were able to determine the values for the $A_{i\mu}$ that were most consistent with our entire 16-observable data set.

We now describe the actual fitting procedure in greater detail. We begin by defining

$$\chi^2 \ \equiv \ \sum_{j,k=1}^{16} \left[F_j - f_j(A_{i\mu})\right] W_{jk} \left[F_k - f_k(A_{i\mu})\right] \ , \tag{22}$$

where F_j are the measured values for the 16 observables, and f_j are the expressions given in the previous section for these same observables in terms of the $A_{i\mu}$'s. In this equation, W_{jk} is the weight matrix, given by

$$W_{jk} \;=\; [\epsilon^{-1}]_{jk}\ . \tag{23}$$

Here ϵ is the full error matrix associated with the set of observables. In the absence of any correlations among the observables, i.e., if each of the observables had been determined independently, W_{jk} would be diagonal, with each element equal to the inverse of the square of the error assigned to each observable,

$$W_{jj} \;=\; \frac{1}{\delta F_j^2}\ . \tag{24}$$

In this work, however, W_{jk} has been generalized to include known correlations (off-diagonal elements) between specific observables, given their method of determination [12]. For example, the values obtained for the in-plane coincident cross-section coefficients, B/A and C/A, were deduced from the same data set by fitting sinusoidal functions to the measured photon yields. Thus, the resulting coefficients of the fit are highly correlated.

The minimization procedure we employed uses a combination of algorithms [14] to locate the minima of an arbitrary, nonlinear function in an arbitrarily large parameter space. The χ^2 function (Eq. 22) can be linearized around a minimum value χ_0^2 via

$$\chi^2 \;=\; \chi_0^2 \;+\; \sum_{\mu=1}^{11} \left.\frac{\partial\chi^2}{\partial A_\mu}\right|_{A_0} \delta A_\mu\ . \tag{25}$$

In this and following equations, we have simplified our notation by denoting all $A_{i\mu}$ with a single index, A_μ, representing either a magnitude or phase. In the above equation, A_0 is the *set* of A_μ values which minimize χ^2, i.e., their values at $\chi^2 = \chi_0^2$. Thus, our minimization condition can be defined by

$$\frac{\partial\chi^2}{\partial A_\nu} \;=\; \left.\frac{\partial\chi^2}{\partial A_\nu}\right|_{A_0} \;+\; \sum_{\mu=1}^{11} \left.\frac{\partial^2\chi^2}{\partial A_\nu \partial A_\mu}\right|_{A_0} \delta A_\mu \;=\; 0\ . \tag{26}$$

Once initial values for the A_μ's are chosen, the parameter search begins by solving for optimal changes in the parameters, δA_μ, then generating new values for these parameters via

$$A_\mu \;=\; A_\mu^{\text{init}} \;+\; \delta A_\mu\ , \tag{27}$$

from which point the parameter search can begin again. This procedure is repeated until a minimum in χ^2 is found.

The minimization condition can be written as a matrix equation

$$\alpha\,\overrightarrow{\delta A} \;=\; \overrightarrow{\beta} \tag{28}$$

or

$$\overrightarrow{\delta A} \;=\; \alpha^{-1}\overrightarrow{\beta} \tag{29}$$

where

$$\alpha_{\mu\nu} \;\equiv\; \frac{1}{2}\,\frac{\partial^2\chi^2}{\partial A_\mu \partial A_\nu}\bigg|_{A_0} \tag{30}$$

and

$$\beta_\mu \;=\; -\frac{1}{2}\,\frac{\partial\chi^2}{\partial A_\mu}\bigg|_{A_0} \quad . \tag{31}$$

The algorithm [14] used to find the χ^2 minimum utilizes a gradient search in the early stages of the fitting process, which transforms smoothly into a linearization of the fitting function as the fit converges. This is achieved by introducing a parameter λ which sets the scale for the size of steps taken along the gradient. To do so, the diagonal elements of the curvature matrix α defined above are modified according to

$$\alpha_{\mu\mu} \rightarrow \alpha'_{\mu\mu} \;=\; (1+\lambda)\,\alpha_{\mu\mu} \;. \tag{32}$$

Upon inspection of this equation, we note that if $\lambda \gg 1$, then

$$\delta A_\mu \;\approx\; \frac{1}{\lambda\,\alpha_{\mu\mu}}\beta_\mu \tag{33}$$

and the search is approximately a gradient search. If, on the other hand, $\lambda \ll 1$, then

$$\alpha'_{\mu\nu} \;\approx\; \alpha_{\mu\nu} \tag{34}$$

and so the function χ^2 is (approximately) linearized, as described in Eqs. 25 and 26. The algorithm is designed such that the closer χ^2 gets to a minimum (determined by the size of the changes in the fitting parameters required to 'step across' the minimum), the smaller the value of λ chosen, and thus a transition from a gradient search to a linearization of χ^2 is effected.

At each scattering angle, a total of 10,000 randomly chosen sets of the A_μ's were used as starting points to this algorithm. Approximately 95% of the time, the algorithm was successful and converged on a minimum in the multi-dimensional χ^2 surface. It quickly became clear, however, that the χ^2 function describing these observables contained many local minima, and the fit would often become 'trapped' in these shallower regions, rather than converging on the 'true' minimum value, $\chi^2_{\rm best}$. (This latter quantity was defined as simply the lowest value of $\chi^2_{\rm min}$ determined in any of the 10,000 fits.) As a result, the algorithm was able to locate minima with $\chi^2_{min} \leq 2\,\chi^2_{\rm best}$ only about 10% of the time, an indication of the complexity of the space being probed. Nevertheless, this yielded a sample of roughly 1000 sets of amplitudes at each angle which gave reasonably good descriptions of all 16 measured observables.

The procedures used to extract final values for each spin-operator amplitude will be presented in the next section. For now, we note that within these 1000 or so acceptable solutions, the *magnitudes* of the amplitudes, $|A_{i\mu}|$, were generally found to be very stable, and largely independent of the choice of starting parameters. The values found for the corresponding *phases*, $\phi_{i\mu}$, on the other hand, were highly dependent on the starting parameters, and thus exhibited much larger fit-to-fit variations. Based on this, a second round of fitting was undertaken, in which the starting parameters were *not* chosen at random: in this analysis, the magnitudes were initially set to their best-fit values, as determined from the first round of fitting, while the phases were each stepped through all allowed values in a multi-dimensional grid search. Specifically, each phase was assigned a starting value between 0 and $5\pi/3$ in steps of $\pi/3$, with all possible combinations used as starting sets.

As a final check on the robustness of the entire fitting procedure, we used a set of theoretical amplitudes (see Sect. VI) to generate values for each of the observables that had been measured in Ref. [12], thereby producing a 'data set' comparable to that obtained in the actual measurement. Using this 'data' as input to our fitting code, we were indeed able to reproduce the input amplitudes, i.e., the algorithm could always find the correct solution. Once this had been established, we performed a more realistic test in which the calculated value of each observable was randomized with a root-mean-square deviation σ equal to a typical experimental error bar for that observable. Using this data set, whose statistical precision matched that of the actual measurements, we were again able to reproduce our input amplitudes, within acceptable errors.

V. RESULTS OF THE FITTING

After performing 10,000 fits to the data at each scattering angle, our next step was to try to converge on a unique set of solutions for the $A_{i\mu}$'s. At each angle, we first discarded all fits in which the resulting χ^2 minimum, $\chi^2_{\rm min}$, was more than twice the lowest value found, $\chi^2_{\rm best}$. For the number of degrees of freedom in our fitting function, this provided a confidence level of 85% that the true solution was included among the 1000 or so fits kept at each angle [15]. Among these 1000 fits, though, the solutions tended to cluster tightly around a very small number of regions in parameter space, yielding a set of roughly 5–10 distinct solutions for each angle. As mentioned previously, the amplitudes extracted from these different solutions were often quite similar in magnitude, but showed discrete (and correlated) variations in phase.

To proceed further, i.e., to select from among these few distinct sets of solutions, it was necessary to introduce additional assumptions concerning the angle dependence of the amplitudes. By imposing the constraint that the amplitudes vary slowly and smoothly as a function of momentum transfer (as do all the observables described by these amplitudes), we were able to eliminate most of the remaining ambiguities in the values determined for the $A_{i\mu}$'s. We will illustrate this procedure with examples below. Before invoking such arguments, it is important to note that as the magnitude of a complex quantity goes through a minimum, both the real *and* the imaginary components must pass close to zero; hence the phase will typically change by roughly 180° as one passes through this minimum. Conversely, it is difficult to produce such a large phase shift *unless* a magnitude becomes very small.

We now examine in detail the two amplitudes A_{nn} and A_{KK}. Shown in Fig. 1 are the fitted magnitudes and the relative phase of these two amplitudes, each plotted versus the center-of-mass scattering angle. (For plotting purposes, all phases lie in the range $-180^\circ \leq \phi_{i\mu} \leq 180^\circ$.) Different plotting symbols at each angle correspond to different sets of solutions, and have been displaced slightly in angle. The magnitudes of both A_{nn} and A_{KK} are large over the range $5^\circ \leq \theta_{\rm c.m.} \leq 13^\circ$ for all valid solutions, and decrease smoothly with angle. The phase difference $(\phi_{nn} - \phi_{KK})$ is close to zero everywhere *except* for a single solution at $\theta_{\text{c.m.}} = 8.8^\circ$, indicated by a daggered 'X', which is near -180°. If one assumes that neither A_{nn} nor A_{KK} passes near zero in this region, then this phase, and all other fitted values associated with this solution, are almost certainly unphysical. While one could attempt to make this argument more quantitative, e.g., by fitting the magnitudes of A_{nn} and A_{KK} with simple functions that did or did not pass near zero somewhere in this angle range, we feel that even a cursory examination of Fig. 1 tends to rule out the possibility of a zero-crossing. These arguments will become even stronger (though obviously somewhat more model-dependent) when we compare our results to a wide range of realistic theoretical predictions for these quantities, all of which display very smooth variations over this range of momentum transfer.

It is interesting to note that the three quantities presented in Fig. 1 largely determine the observable D_{0q}, which in the direction $\hat{\mathbf{k}} \cdot \hat{\mathbf{n}} = \hat{\mathbf{k}} \cdot \hat{\mathbf{K}} = 1/\sqrt{2}$, $\hat{\mathbf{k}} \cdot \hat{\mathbf{q}} = 0$ has the value

$$D_{0q} \approx \Im(A_{nn}A^*_{KK}) = |A_{nn}||A_{KK}| \sin(\phi_{nn} - \phi_{KK}) \ . \tag{35}$$

Our measured value for this observable, being close to zero, drives the phase difference to either zero or 180°, but supplies little additional information to the fit. Constraints on the magnitudes of A_{nn} and A_{KK}, and the resolution of this 180° phase ambiguity, must therefore be supplied by other observables, demonstrating again the advantages of a large, diverse data set.

By applying similar arguments to other $A_{i\mu}$'s, we were able to eliminate most of the remaining solution sets, and arrive at a nearly ambiguity-free determination of the magnitude and phase of each amplitude at all angles. For most quantities, the few distinct solutions left were sufficiently close in value that a simple average could be taken, with errors enlarged slightly to reflect the range of solutions included. Exceptions to this behavior occurred only at $\theta_{\text{c.m.}} = 16.5^\circ$, where two of the phase differences exhibited two-fold discrete ambiguities that could not be resolved; an interpretation for this will be given in the following section. In all cases, the final values determined for the $A_{i\mu}$ magnitudes and phases were consistent with those found in the fits which yielded the lowest minimum for χ^2, denoted here by χ^2_{best}.

As the final step in our analysis, the values obtained for χ^2_{best} were normalized to the number of degrees of freedom in the fit, to yield χ^2_ν, a quantity which statistically should lie close to unity. In this work, the values for χ^2_ν at $\theta_{\text{c.m.}} = 5.5^\circ$, 8.8°, 12.1°, and 16.5° were 0.75, 2.14, 2.17, and 6.47, respectively. Because the fitting function should provide an accurate description of the data (that is, one is *not* gauging the appropriateness of the model in this case), a minimum χ^2_ν in substantial excess of 1 suggests an underestimate of the input error for at least part of the fitted data set. To compensate for this, the error determined in the fitting process for the magnitudes and phases of each of the $A_{i\mu}$'s was artificially increased by a factor of $\sqrt{\chi^2_\nu}$. This ensures that when the extracted amplitudes are used to determine best-fit values (with errors) for the observables, one will reproduce the measured input data within one standard deviation, on average. Thus, we believe that the errors quoted here for the magnitudes and phases of the $A_{i\mu}$'s provide a realistic estimate of the true uncertainties inherent in the fits to these data.

VI. COMPARISON OF AMPLITUDES WITH CALCULATIONS

It has been shown previously [12] that the large number of spin observables measured for this transition provides a severe test for any theoretical model. None of the calculations presented in Ref. [12] could describe the momentum transfer dependence of all the observables over the entire range covered by the data. To determine more precisely where weaknesses lie in these models, it is useful to bring experiment ‘closer’ to theory by comparing not the measured observables, as was done in Ref. [12] but by comparing theoretical predictions for the $A_{i\mu}$ amplitudes with values extracted directly from the data, as described here.

In this work, we will consider five different sets of predictions for the scattering amplitude. To carry out these calculations, many details must be specified, such as: the method used to generate the distorting potential, and how well this describes the elastic scattering data; assumptions made regarding the structure of the excited state; the extent to which medium corrections are incorporated into the effective interaction; the handling of exchange contributions to the interaction; etc. Here, we will examine predictions for the $A_{i\mu}$'s derived from the *same* five models as those to which the *observables* were compared in Ref. [12]. Extensive discussion on the content of each calculation is presented in that paper, and the interested reader is encouraged to refer to Ref. [12] for more detail; only fairly brief descriptions will be provided here.

Of the five calculations to be shown, all use free t-matrices for the effective interaction, and Cohen-Kurath matrix elements [16] to specify the transition to the excited state. Two are relativistic calculations in which both direct and exchange contributions are included explicitly (DREX) [17]. The distorting potential for the incident and outgoing projectile waves, however, is generated either “self-consistently” (the same interaction that induces the $0^+ \rightarrow 1^+$ transition is also folded with the ^{12}C ground state transition density to produce the distortions), or from an optical potential, with parameters fit to p+^{12}C elastic scattering cross section and analyzing power data. In all of the figures, the predictions of these two calculations will be shown as a solid line (self-consistent) and a long-dashed line (optical potential). Two nonrelativistic calculations also include both direct and exchange contributions explicitly (DW81) [18], and also incorporate the effects of distortion using the same two methods, i.e., either self-consistently (dotted line) or from the same optical potential as was used in the relativistic calculation (dot-dashed line). Finally, we will compare our values of the scattering amplitudes to those predicted using a relativistic calculation in which the full interaction has been parameterized in terms of direct scattering processes *only*, with distorted waves generated self-consistently (short-dashed line). Although exchange processes are expected to contribute significantly to this reaction, this last calculation appeared to describe the *observables* measured for this reaction better than any model in which exchange contributions had been explicitly included [12]. This would suggest that most current methods of accounting for exchange processes are inadequate to describe proton-nucleus scattering at intermediate energies, at least for unnatural parity transitions.

Before making detailed comparisons between data and theory, there is one ambiguity which must be pointed out. Because the individual spin-operator amplitudes have dimensions of $\sqrt{\mu\mathrm{b/sr}^2}$, cross section data [13] were used to provide an overall normalization factor for all spin observables considered in the fitting procedure. This ensures, for example, that

Eq. 8 is obeyed, and the sum of the squared amplitudes equals the measured cross section. However, as can be seen in Fig. 2, the five calculations considered here do not reproduce this cross section. In particular, all of the calculations underpredict $d\sigma/d\Omega_p$ at small angles, except for the DW81 calculation using distortions generated in an optical model, which overpredicts the data at small angles, then decreases much more rapidly with angle than the data. The DW81 calculation which uses self-consistent distortions, on the other hand, is a much more shallow function of angle than the data suggest.

In light of these discrepancies, one could consider scaling all of the calculated magnitudes, $|A_{i\mu}|$, by a single multiplicative factor, in order to more closely reproduce the measured cross section. In this way, one is effectively comparing the *relative* sizes of the spin-operator amplitudes for each model to the measured values. This also ensures that the dominant amplitudes will be well reproduced. On the other hand, the differences observed between the predicted and measured cross sections might result from particular amplitudes (especially the larger ones) being grossly over- or under-predicted, while the calculated values for others are actually in close agreement with the experimentally determined values. In this case, one is best served by *not* applying an artificial normalization, and directly comparing data and theory for each amplitude. Because our primary goal is to identify more narrowly the weaknesses in individual calculations, we have adopted the latter approach here. The potential drawback, of course, is that a calculation that is correct in all respects other than reproducing the measured cross section will systematically miss *each* of the extracted amplitudes by roughly the same factor.

With the above caveat in mind, we now compare the predictions of these five models for the magnitude and phase of each amplitude to the values deduced from our fits. The quantity A_{n0}, shown in Fig. 3, is the amplitude for polarizing the recoil ^{12}C nucleus along the $\hat{\mathbf{n}}$ direction (perpendicular to the scattering plane) with an unpolarized incident proton. Its magnitude (upper plot) is predicted by each calculation to be quite weak over the entire angle range studied in this work, a feature also seen in the data. The differences among the various calculations are, in absolute terms, very small. Thus, given the level of precision with which this quantity can be determined experimentally, not much useful information can be obtained from $|A_{n0}|$, other than confirming the small probability for producing this particular spin configuration. Due to the small size of $|A_{n0}|$, the phase difference $\phi_{n0} - \phi_{nn}$, shown in the lower half of Fig. 3, exhibits a twofold discrete ambiguity at the largest scattering angle. As discussed earlier, if the magnitude of a complex amplitude passes near zero, its phase can change by nearly 180°. Our data suggest that A_{n0} passes near zero (has a local minimum) somewhere around $\theta_{\mathrm{c.m.}} = 16.5°$, but our measurements can not establish this unambiguously. We also note that at smaller angles the phase difference is relatively flat, in agreement with all of the calculations, although the values deduced from the data are significantly more negative (by $\sim 90°$) than any of the calculations predict.

In contrast to this weak amplitude, we next examine A_{nn}, shown in Fig. 4, which is the amplitude for polarizing the recoil nucleus along the $\hat{\mathbf{n}}$ direction when the incident proton is also polarized along $\hat{\mathbf{n}}$. The data show that $|A_{nn}|$ is large throughout the angular range studied, and decreases smoothly with increasing momentum transfer. All five calculations predict this general behavior, but differ significantly in strength, relative to the precision with which this quantity has been determined. It is useful to note the striking similarities between this figure and Fig. 2, the unpolarized cross section. (For a more quantitative comparison, one would need to square the results shown in Fig. 4.) Just as for $d\sigma/d\Omega_p$, the values of $|A_{nn}|$ at small momentum transfer are underpredicted slightly by four of the calculations, and overpredicted by the DW81 calculation which uses optical model distortions. The momentum transfer dependence of the data is reasonably well described by the three relativistic calculations, but is too steep (shallow) for the DW81 calculations that use optical model (self-consistent) distortions. The inabilities of the models to reproduce this particular amplitude are thus directly reflected in the discrepancies found between the predictions and measured values for the scattering cross section.

Similar behavior is seen in Fig. 5 for the other large amplitude, A_{KK}, the amplitude for polarizing the recoil nucleus along the average momentum direction using an incident proton polarized along the same direction. The measured magnitude $|A_{KK}|$ (upper plot), like $|A_{nn}|$, closely follows the angular dependence of the differential cross section, and decreases monotonically with $\theta_{\text{c.m.}}$. In this case, the three relativistic calculations *quantitatively* describe this behavior, and agree with the data at all values of momentum transfer. The two nonrelativistic calculations, on the other hand, do very poorly, either over- or underpredicting the strength of this amplitude at small angles, and predicting angle dependences which are either too steep or too shallow, depending on the method used to generate distortions. Also shown in Fig. 5 is the phase difference $\phi_{nn} - \phi_{KK}$, which is predicted by all of the calculations to be very close to zero over this entire angular range. The data support this idea, albeit with a fairly large statistical uncertainty, suggesting that the two largest amplitudes contributing to this reaction are closely matched in phase.

The third "diagonal" amplitude, A_{qq}, has some intriguing properties. A_{qq} is the amplitude for polarizing the recoil ^{12}C nucleus along the $\mathbf{q}$ (momentum transfer) direction, with the proton also polarized along $\mathbf{q}$, i.e., this amplitude is associated with the spin-operator combination $(\mathbf{\Sigma}\cdot\mathbf{q})(\sigma\cdot\mathbf{q})$. In a meson-exchange formulation of NN scattering [19], the one-pion exchange amplitude is associated with the spin-operator $(\sigma_{\mathbf{1}}\cdot\mathbf{q})(\sigma_{\mathbf{2}}\cdot\mathbf{q})$, which is very similar. Perhaps of more significance, in a relativistic PWIA, A_{qq} is the only amplitude that contains contributions from the pseudovector invariant NN amplitude, which carries the same quantum numbers as the pion. Because the excitation of the 15.11 MeV state is a $\Delta T = 1$ transition, one-π and one-ρ exchange should dominate the reaction process. The potentials for π and ρ exchange interfere constructively at very small momentum transfer, but the one-π exchange term changes sign relative to one-ρ exchange at relatively low momentum transfer [20], which can lead to large cancellations. Thus, a zero crossing in the A_{qq} amplitude may be a direct reflection of $\pi - \rho$ interference in the reaction mechanism for this transition.

Inspection of the extracted values for the magnitude and phase of A_{qq}, plotted in Fig. 6, clearly indicates that this amplitude does indeed cross zero somewhere between $\theta_{\text{c.m.}} = 5.5^\circ$ and 12.1°. The magnitude $|A_{qq}|$, which exhibits a very different q dependence than either $|A_{nn}|$ or $|A_{KK}|$, is very well described by all of the relativistic calculations, which each predict a zero crossing somewhere near $\theta_{\text{c.m.}} \sim 9^\circ$. The data are not described quite as well by the nonrelativistic calculation which uses self-consistently generated distortions, and are in strong disagreement with the other DW81 calculation. The large experimental uncertainty in the phase difference at $\theta_{\text{c.m.}} = 8.8^\circ$ supports the idea that a zero crossing occurs near this point. The two relativistic calculations which have distortions generated self-consistently describe the momentum transfer dependence of both the magnitude and phase of A_{qq} quite well, and thus best describe the physics contained in this amplitude.

The last two amplitudes, the off-diagonal terms A_{Kq} and A_{qK}, are also intriguing. Physically, they represent the amplitudes for polarizing the recoil ^{12}C nucleus along either the **K** or **q** direction when the proton probe is polarized along either the **q** or **K** direction, respectively. In a nonrelativistic PWIA, these two amplitudes should be identically zero for this transition, and only become non-zero if non-local effects, such as knock-on exchange, are explicitly included [6]. In a relativistic formulation, on the other hand, A_{Kq} and A_{qK} include contributions due to linear couplings between the upper and lower components of the bound nucleon wave function, even in PWIA. Because the lower components are momentum-dependent, the nucleon is manifestly off-shell, and non-local effects arise “naturally.” Formally, A_{Kq} and A_{qK} are proportional to the tensor and axial vector pieces of the invariant NN amplitude, respectively. By carrying out the spin algebra [6], these can be written in terms of the composite spin-convection current amplitudes $\langle\sigma \times \mathbf{J}\rangle$ and $\langle\sigma \cdot \mathbf{J}\rangle$, again respectively. Thus, these two amplitudes should be sensitive to the off-shell behavior of the nucleons inside the ^{12}C nucleus.

In Fig. 7, we see that the extracted magnitude of A_{Kq} is significantly smaller than all of the predicted values, especially at small angles. This suggests a quenching of the tensor component of the NN amplitude within the nucleus, though one can not tell if this is a nuclear structure or an interaction effect. It is very curious that the only relativistic calculation that does *not* include exchange (short-dashed line) also predicts the largest magnitude for an amplitude that, at least nonrelativistically, is driven largely by exchange contributions. Unfortunately, little insight is provided by the phase difference, $\phi_{nn} - \phi_{Kq}$. Note, however, that if the phase found at the largest angle is simply shifted by 360°, the general shape of the angular dependence of the phase difference is followed reasonably well by three of the calculations, albeit with a $\sim 90°$ offset.

In striking contrast, the other off-diagonal amplitude, A_{qK}, is predicted to be somewhat smaller than A_{Kq} over most of this angle range, while the experimentally determined values are seen in Fig. 8 to be quite a bit larger. Only the DWIA calculation using optical model distortions is consistent with the typical strength suggested by the data. Figure 8 also shows, though, that the limited statistical precision with which this amplitude has been determined makes it difficult to draw any conclusions about the momentum transfer dependence of this quantity. This limitation is also evident in the phase difference, in which a tight clustering about zero is broken only at the largest angle, where a two-fold discrete ambiguity is observed at 16.5°. As was the case for A_{n0}, our statistical accuracy is such that we cannot determine experimentally whether this amplitude is crossing zero in this angle regime or not. Two calculations predict amplitudes that, in the complex plane, pass near zero on one side ($\Delta\phi = +180°$), two pass on the other side ($-180°$), and one phase remains constant. All of these possibilities are consistent with one of the allowed solutions extracted from the data.

VII. SUMMARY AND CONCLUSIONS

We have made a model-independent determination of the full transition amplitude for the ^{12}C$(p,p')^{12}$C* (15.11 MeV, 1^+, $T = 1$) reaction at an incident beam energy of 200 MeV at four scattering angles. This represents the first such determination for any hadron-induced nuclear transition other than those with $J_i = J_f = 0$. By imposing only loose “smoothness” constraints on the momentum transfer dependence of the individual spin-operator amplitudes, we have performed a nearly ambiguity-free extraction of these quantities, which has provided deeper insight into the physics driving this transition.

As expected theoretically, the two diagonal spin-operator amplitudes A_{nn} and A_{KK} were found to be the dominant amplitudes over the entire momentum transfer range studied. Each of these was better described by the three calculations carried out in relativistic frameworks than by the two nonrelativistic calculations we considered. The third diagonal amplitude, A_{qq}, which has a spin-operator structure similar to that of one-pion exchange, exhibited behavior characteristic of a "zero crossing." The value of momentum transfer at which this occurred was again much better matched by the relativistic calculations than the DWIA predictions. This crossing has physical significance in that it may reflect interference between π and ρ exchange, and hence may serve as a gauge of the relative strengths of these two contributions within the nuclear medium.

The three off-diagonal amplitudes are all much weaker than the three just discussed, and as such were determined with much larger experimental uncertainties. The magnitude of the A_{n0} amplitude provided little insight, though the phase was consistently (i.e., at all angles) off by about 90° relative to most of the predicted values. The amplitudes A_{Kq} and A_{qK} are expected to be sensitive to the off-shell behavior of the nucleons inside the ^{12}C nucleus, and should therefore probe the non-local or exchange nature of the scattering process. Despite the sizable errors on the experimentally determined values for these two amplitudes, neither are described well by any of the five calculations considered here, which may indicate problems in our present treatment of non-local effects in both relativistic and non-relativistic frameworks.

ACKNOWLEDGEMENTS

We thank those who participated in the experiment from which the observables discussed here were obtained. We also thank J. Piekarewicz and J. R. Shepard for providing us with the calculations and for useful discussions.

This work was supported in part by the US National Science Foundation under Grant No. PHY-9602872.

REFERENCES

* Present address: Center for Applied Physics Studies, Louisiana Tech University, Ruston, Louisiana 71272.

[1] See, for example, H. Baghaei *et al.*, Phys. Rev. Lett. **69**, 2054 (1992), and references therein.

[2] W. G. Love, A. Klein, and M. A. Franey, in *Antinucleon- and Nucleon-Nucleus Interactions*, edited by G. E. Walker, C. D. Goodman, and C. Olmer (Plenum, New York, 1985), p. 1.

[3] T. A. Carey, J. M. Moss, S. J. Seestrom-Morris, A. D. Bacher, D. W. Miller, H. Nann, C. Olmer, P. Schwandt, E. J. Stephenson, and W. G. Love, Phys. Rev. Lett. **49**, 266 (1982).

[4] K. H. Hicks *et al.,* Phys. Lett. B **201**, 29 (1988).

[5] W. G. Love and J. R. Comfort, Phys. Rev. C **29**, 2135 (1984) and references therein.

[6] J. Piekarewicz, R. D. Amado, and D. A. Sparrow, Phys. Rev. C **32**, 949 (1985).

[7] J. R. Shepard, E. Rost, and J. A. McNeil, Phys. Rev. C **33**, 634 (1986).

[8] J. M. Moss, Phys. Rev. C **26**, 727 (1982).

[9] E. Bleszynski, M. Bleszynski, and C. A. Witten, Phys. Rev. C **26**, 2063 (1982).

[10] J. Piekarewicz, E. Rost, and J. R. Shepard, Phys. Rev. C **41**, 2277 (1990).

[11] G. Ramachandran, A. R. Usha Devi, and A. Sudha Rao, Phys. Rev. C **49**, R623 (1994).

[12] S. P. Wells *et al.,* Phys. Rev. C **52**, 2559 (1995).

[13] J. R. Comfort, R. E. Segel, G. L. Moake, D. W. Miller, and W. G. Love, Phys. Rev. C **23**, 1858 (1981).

[14] Philip R. Bevington, *Data Reduction and Error Analysis for the Physical Sciences*, McGraw-Hill, New York (1969).

[15] I. N. Bronshtein and K. S. Semendyayev, *Handbook of Mathematics,* Van Nostrand Reinhold Company, New York (1985).

[16] S. Cohen and D. Kurath, Nucl. Phys. **73**, 1 (1965); T. H. S. Lee and D. Kurath, Phys. Rev. C **21**, 293 (1980).

[17] E. Rost and J. R. Shepard, computer code DREX, unpublished; E. Rost and J. R. Shepard, Phys. Rev. C **35**, 681 (1987).

[18] R. Schaeffer and J. Raynal, Saclay Report No. CEA-R4000, 1970; modifications by J. R. Comfort.

[19] V. G. J. Stoks, R.A.M. Klomp, M.C.M. Rentmeester, and J.J. de Swart, Phys. Rev. C **46**, 792 (1993).

[20] C. J. Horowitz and J. Piekarewicz, Phys. Rev. C **50**, 2540 (1994).

FIGURES

FIG. 1. Sets of fitted values for the magnitudes of A_{nn} *(top)* and A_{KK} *(middle)*, and their relative phase difference *(bottom)*, each plotted vs. $\theta_{\mathrm{c.m.}}$. In each case, different plotting symbols at each angle represent the results of different solutions. The symbols have been displaced slightly in angle for (some) clarity.

FIG. 2. Differential cross section for the $^{12}\mathrm{C}(p,p')^{12}\mathrm{C}^*$ (15.11 MeV) reaction at 200 MeV. The data are from Ref. [13]. The five curves shown are described in the text.

FIG. 3. Magnitude *(upper)* and relative phase *(lower)* of the amplitude A_{n0} plotted vs. the center of mass scattering angle. The phase difference is with respect to the A_{nn} amplitude. The error bands represent best fit solutions to the data of Ref. [12]. The five curves shown are theoretical predictions described in the text.

FIG. 4. Same as Fig. 3, but for the amplitude A_{nn}. In our fitting procedures, the phase of this amplitude was defined to be zero.

FIG. 5. Same as Fig. 3, but for the amplitude A_{KK}.

FIG. 6. Same as Fig. 3, but for the amplitude A_{qq}.

FIG. 7. Same as Fig. 3, but for the amplitude A_{Kq}.

FIG. 8. Same as Fig. 3, but for the amplitude A_{qK}.

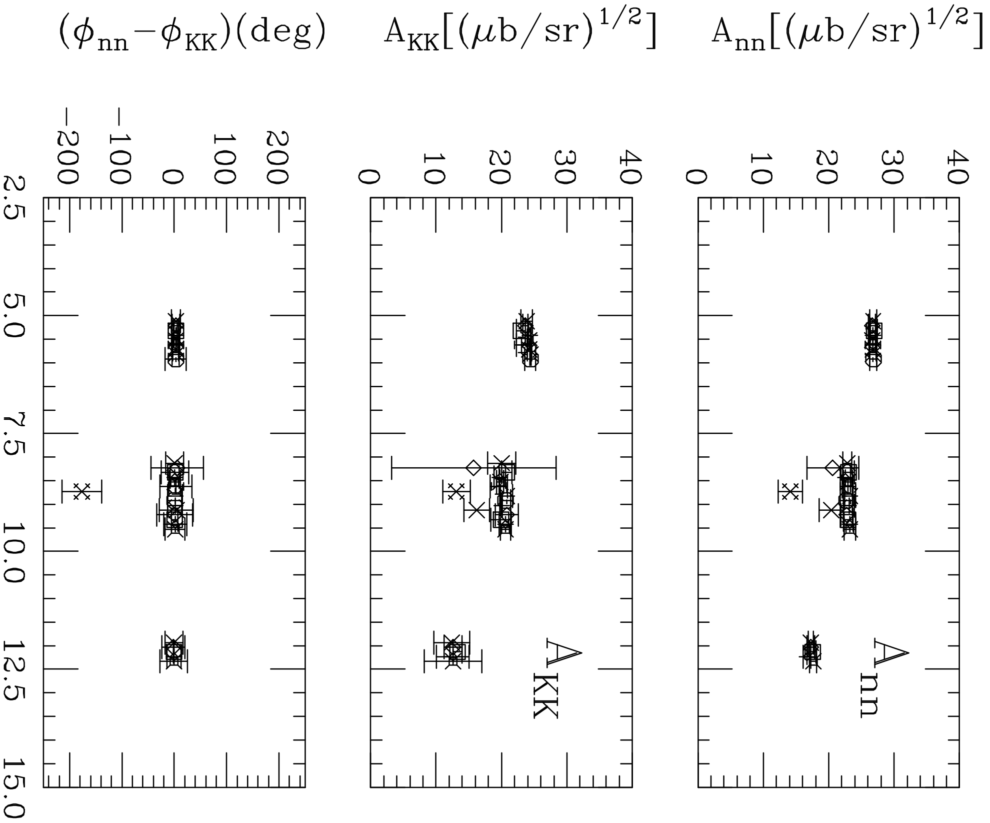
Ann[(μb/sr)^1/2]
AKK[(μb/sr)^1/2]
(φnn−φKK)(deg)
θc.m. (deg)
Ann
AKK
0
10
20
30
40
−200
−100
0
100
200
2.5
5.0
7.5
10.0
12.5
15.0

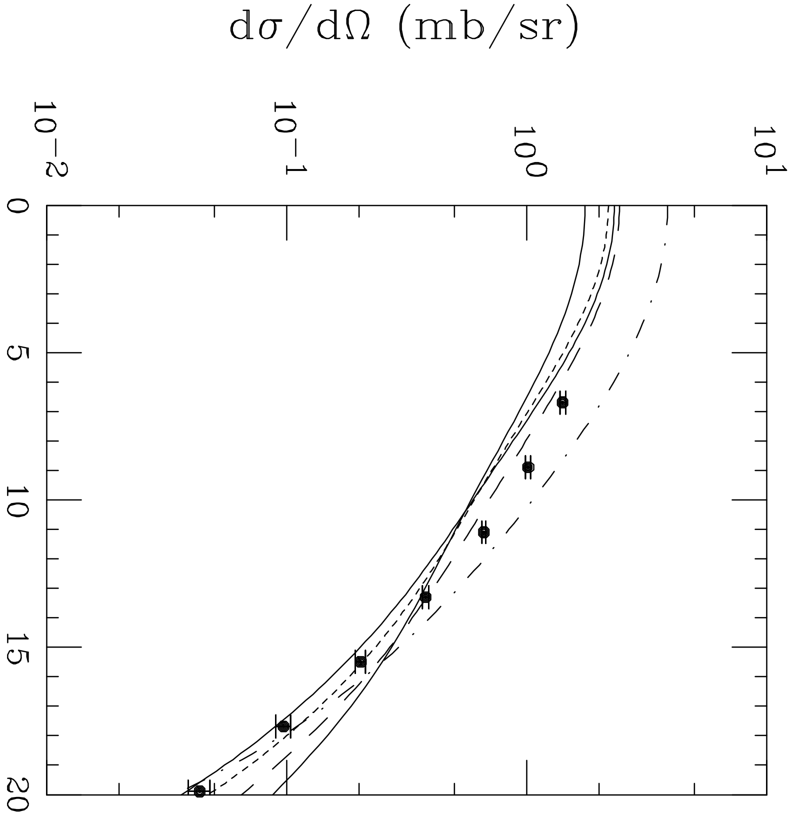
dσ/dΩ (mb/sr)
10^{-2}
10^{-1}
10^{0}
10^{1}
$\theta_{\rm c.m.}$ (deg)
0
5
10
15
20

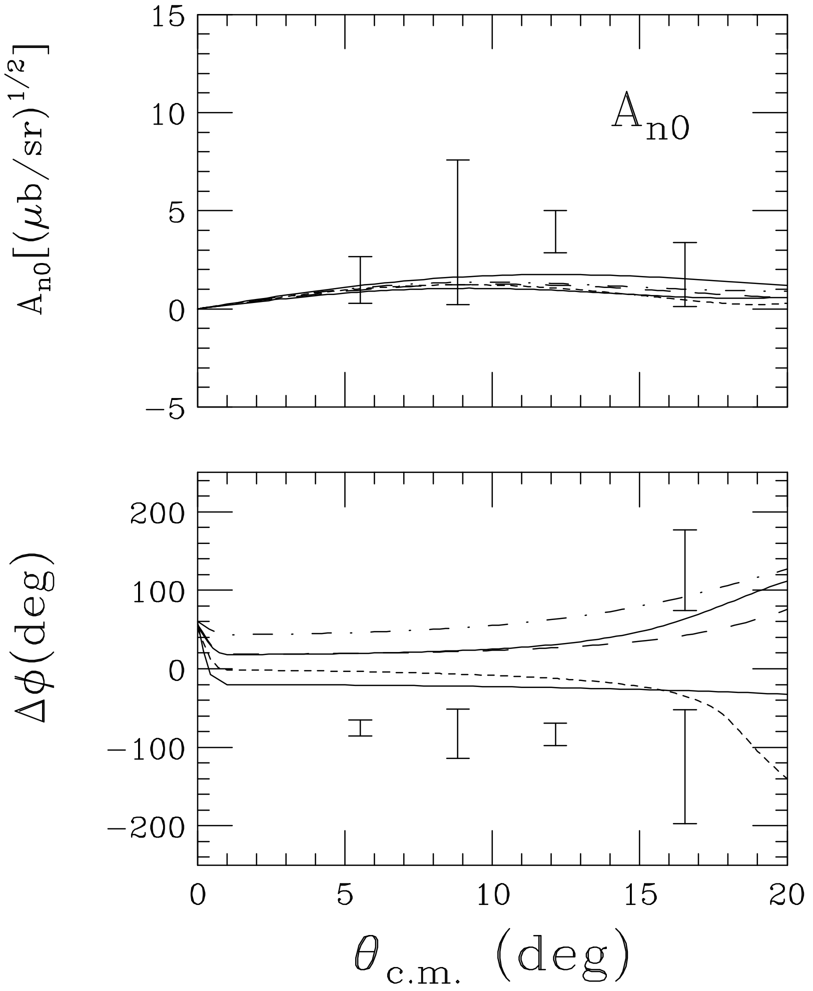

15
10
5
0
−5
$A_{n0}[(\mu b/sr)^{1/2}]$
A_{n0}
200
100
0
−100
−200
$\Delta\phi$(deg)
0
5
10
15
20
$\theta_{c.m.}$ (deg)

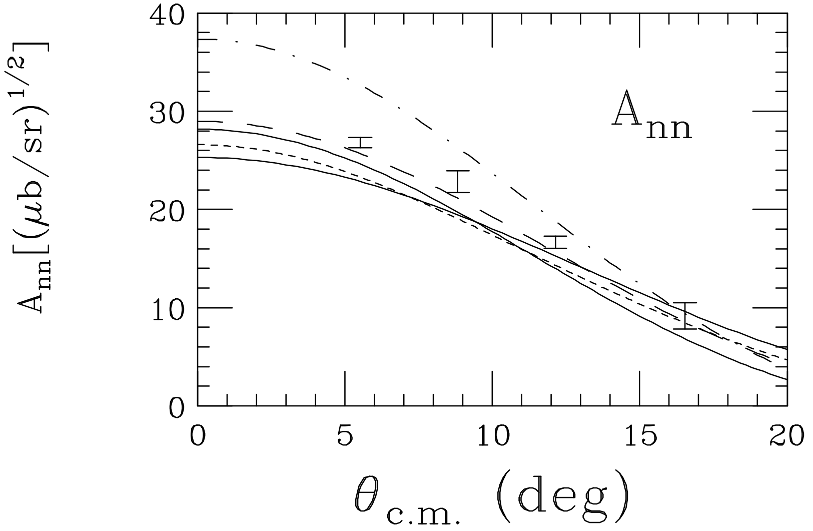
A$_{nn}$
$A_{nn}[(\mu b/sr)^{1/2}]$
0
10
20
30
40
0
5
10
15
20
$\theta_{c.m.}$ (deg)

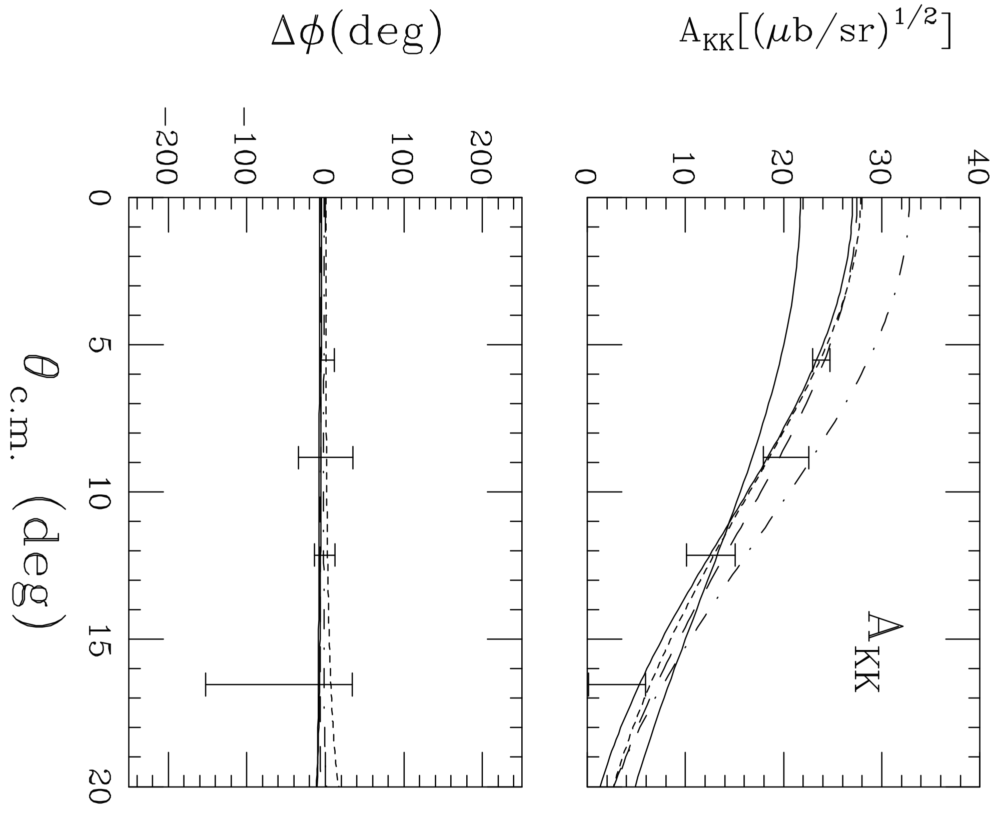

$A_{KK}[(\mu b/sr)^{1/2}]$
0
10
20
30
40
A_{KK}
$\Delta\phi$(deg)
−200
−100
0
100
200
0
5
10
15
20
$\theta_{c.m.}$ (deg)

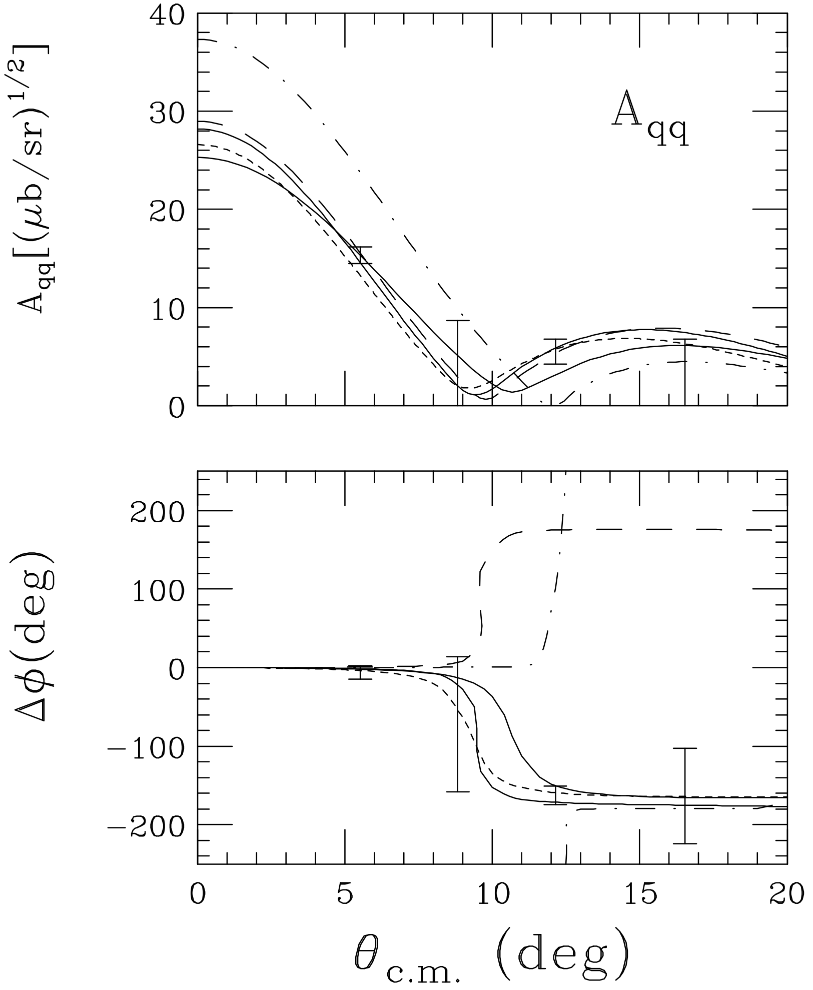
$A_{qq}[(\mu b/sr)^{1/2}]$
A_{qq}
40
30
20
10
0
$\Delta\phi$(deg)
200
100
0
−100
−200
0
5
10
15
20
$\theta_{c.m.}$ (deg)

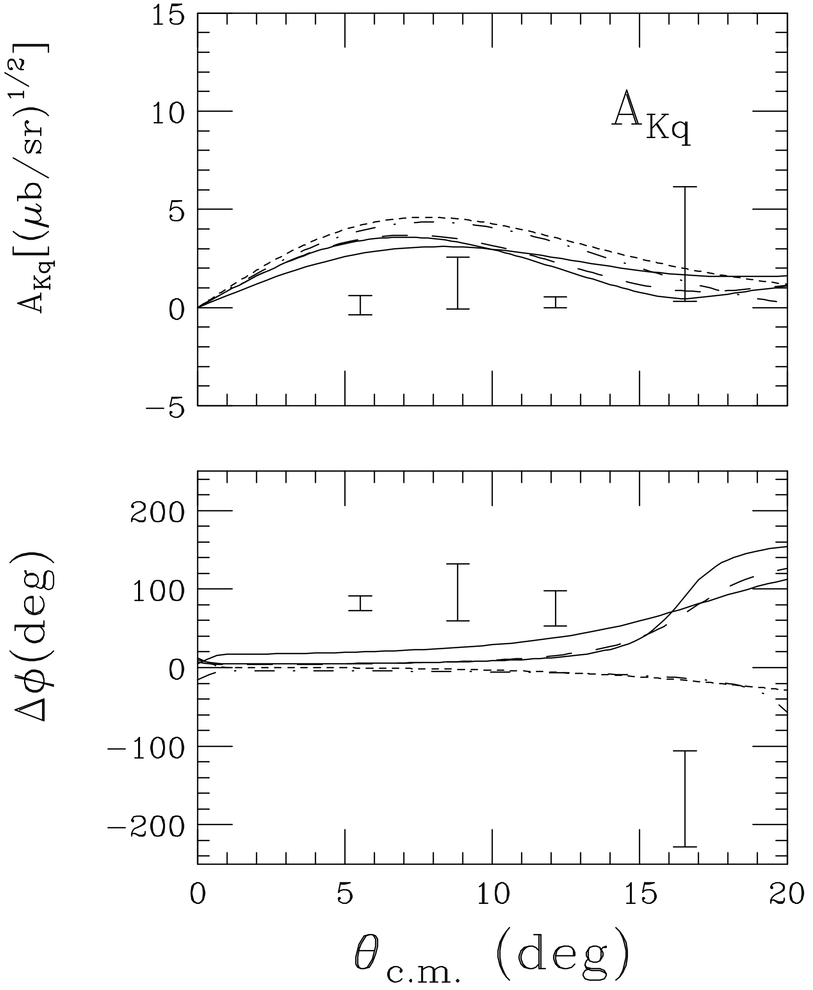
$A_{Kq}[(\mu b/sr)^{1/2}]$
A_{Kq}
15
10
5
0
−5
$\Delta\phi$(deg)
200
100
0
−100
−200
0
5
10
15
20
$\theta_{c.m.}$ (deg)

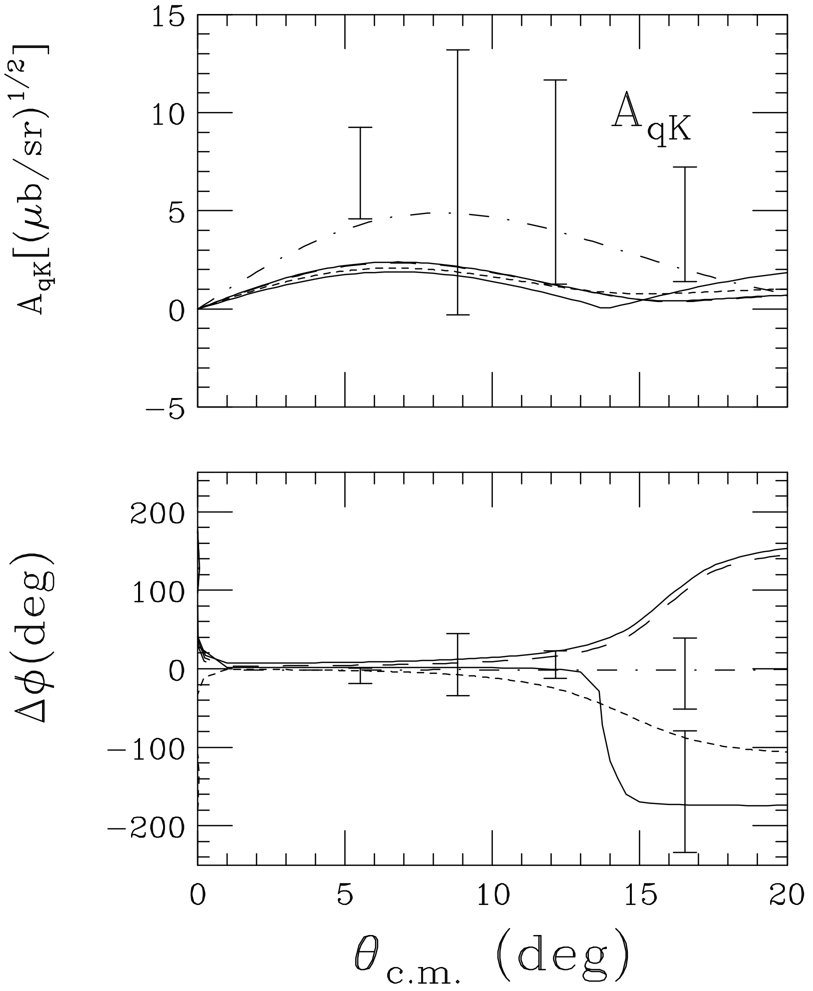
A_qK
$A_{qK}[(\mu b/sr)^{1/2}]$
15
10
5
0
−5
$\Delta\phi$(deg)
200
100
0
−100
−200
0
5
10
15
20
$\theta_{c.m.}$ (deg)